PCCP

Accepted Manuscript

ROYAL SOCIETY OF CHEMISTRY

www.rsc.org/pccp

Journal Name

ARTICL

Microwave Spectroscopic and Theoretical Investigations of the Strongly Hydrogen Bonded Hexafluoroisopropanol•••Water Complex

Received 00th January 20xx,
Accepted 00th January 20xx

DOI: 10.1039/x0xx00000x

www.rsc.org/

A. Shahi,[a] E. Arunan[a]

This paper reports microwave spectroscopic and theoretical investigations on the interaction of water with hexafluoroisopropanol (HFIP). The HFIP monomer can exist in two conformations, antiperiplanar (AP) and synclinical (SC). The former is about 5 kJ mol^{-1} more stable than the later. Theoretical calculations predicted three potential minima for the complex, two having AP and one having SC. Though, the binding energy for the HFIP(SC)•••H_2O turned out to be larger than that for the other two conformers having HFIP in the AP form, the global minimum for the complex in the potential energy hypersurface had HFIP in the AP form. Experimental rotational constants for four isotopologues measured using a pulsed nozzle Fourier transform microwave spectrometer, correspond to the global minimum in the potential energy hypersurface. Structural parameters and the internal dynamics of the complex could be determined from the rotational spectra of the four isotopologues. The global minimum has the HFIP(AP) as hydrogen bond donor forming a strong hydrogen bond with H_2O. To characterize the strength of the bonding and to probe the other interactions within the complex, atoms in molecules, non-covalent interaction index and natural bond orbital theoretical analyses have been performed.

Introduction

It is unquestionable that hydrogen bonding is the most important among all the known weak interactions. In daily life, aliphatic alcohols play an important role by forming hydrogen bonds. Water (H_2O), methanol (CH_3OH) and ethanol (C_2H_5OH) are the first three "alcohols" having entirely different effects on the human body. In recent years, it has been found that fluorinated aliphatic alcohols possess unique properties. The titled fluorinated aliphatic alcohol, hexafluoroisopropanol (HFIP) is an important solvent for organic chemists, polymer chemists and biologists. The aqueous solution of HFIP or other fluoroalcohols, trifluoroethanol (TFE) helps in stabilizing the α-helical structure of protein.[1–4] Interestingly, HFIP is able to dissolve, the hard-to-dissolve polymers (*e.g.* Polyethylene terephthalate) at room temperature because it forms strong hydrogen bonds. Therefore, polymers should have hydrogen bond acceptor groups *e.g.* polyester, polyamides.[5] HFIP can work as a suitable solvent for rearrangement via zwitterionic intermediate, whereas CH_3OH solvent fails to do that for certain reactions.[6] In aqueous solution, interaction between HFIP molecules and water molecules is difficult to understand because of the fact that there is competition between HFIP-water interaction and HFIP aggregation which depends on the mole fraction of HFIP.[7] The interaction between HFIP and water in the condensed phase has been investigated by FTIR-ATR, IR, Raman, X-ray diffraction, small angle neutron scattering, NMR, mass spectrometry and molecular simulation studies.[7,8] We have studied the HFIP monomer using microwave spectroscopy early. Rotational spectra of the monomer and its five isotopologues confirmed that the molecule exists only in the antiperiplanar (AP) form in supersonic expansion.[9] In this work, we investigate the interaction between HFIP and water in the gas phase using microwave spectroscopy.

One unit of the HFIP•••water complex, water, is well known and its structure is well established. However, spectroscopic and structural properties of the other unit, HFIP, have been the subject of several recent studies.[10–14] Conformational preference of HFIP is very interesting. IR, Raman and matrix isolation studies show that the molecule exists in two conformation; antiperiplanar (AP) and synclinal (SC) (Figure 1). In gas phase, the AP conformer is more stable than the SC conformer.[12,13,15]

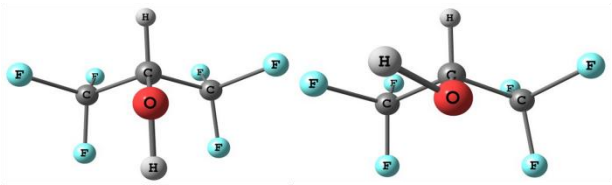

Figure 1. Two conformers of HFIP; antiperiplanar (left side) and synclinical (right side).

[a] *Department of Inorganic and Physical Chemistry, Indian Institute of Science, Bangalore, India, 560012. E-mail: shahi@ipc.iisc.ernet.in*

† Electronic Supplementary Information (ESI) available: See

DOI: 10.1039/x0xx00000x

In CO and N_2 matrices, both the conformers of HFIP have been observed. However, in argon matrix, only the AP conformer could be observed.[12] Relative intensity of these conformers vary with temperature. These conformers arise due to an internal motion of the –OH group. The energy difference between these two conformers is 5.02 kJ mol^{-1} but there is a barrier of 11.29 kJ mol^{-1} for the AP to SC interchange.[9] A prototype molecule, isopropanol, also exists in two isomeric forms because of the –OH internal rotation. However, for this molecule the SC conformer is more stable than the AP.[13,16,17] Examination of the effect of fluorination on isopropanol molecule has been done by Suhm's group, extensively.[13] Other prototype molecules hexafluoroisobutene[18] and hexafluoroacetone imine[19] show a doublet in the rotational spectrum because of the counter motion of opposite CF_3 groups. However, HFIP did not show any splitting. These patterns and the reasons behind them have been discussed in our previous work.[9] In this work, rotational spectrum of the HFIP•••H_2O complex has been discussed. Results from ab initio and density functional theory (DFT) calculations are reported. Moreover, wavefunctiosn from these calculations have been analyzed using atoms in molecules (AIM)[20,21], natural bond orbital (NBO)[22], non-covalent interaction (NCI)[23] index and natural resonance theory (NRT)[24–26] methods as well.

Computational and Experimental Methods

To guess the geometry of the complex, electrostatic potential (ESP) calculations have often been useful.[27,28] First, we analyzed the electrostatic potential of HFIP and H_2O to guess the different possible initial geometries of the HFIP•••water complex (See Figure S1 and Table S1-S4, †ESI). Surface maxima and minima of ESP could be located at the periphery of the molecule (i.e. at 0.001 a.u. surface) using the Multiwfn program.[29,30] The minima are the nucleophilic sites of the molecule and the maxima are the electrophilic sites of the molecule. The guess geometries were considered in such a way that the electrophilic site of HFIP interacts with the nucleophilic site of H_2O and vice versa. Optimization of the different guess structures of the HFIP•••H_2O complex was done using the G09 suite of program.[31] Different ab initio and DFT methods were used for the calculation *e.g.* LC-wPBE/6-311++G(d,p),[32] MP2/6-311++G(d,p), B2PLYP/6-311++G(d,p), CAM-B3LYP/6-311++G(d,p) and wB97XD/6-311++G(d,p).[33,34] Binding energies of the different complexes were calculated using supermolecular approach i.e. binding energy is the difference between total electronic energy of the complex and the sum of the total energies of the monomers (Table 1). Basis set superposition error was corrected from the binding energy using counterpoise method in-built in G09. Moreover, comparisons of electronic energy of different conformers have also been done. This led to a surprising result, which has been discussed in the next section.

Semi-rigid rotor Watson's asymmetric Hamiltonian was used to fit the experimentally observed transitions for rotational and distortion constants,[35] using ASFIT and/or SPFIT programs.[36–38] Calculation of the distortion constants and vibrationally averaged geometry were done using FREQ=VIBROT and FREQ=ANHARMONIC keyword in G09 program. AIM calculations have been performed to characterize the weak interaction using AIMAll program.[39] The results gave some unexpected bond critical points (BCPs) for intermolecular interaction. These were further confirmed using NCI index plots.[23] To determine the orbital overlaps between bonded atoms, NBO analysis has been done using NBO 6.0 software.[40] Contribution of covalency and ionicity of the hydrogen bond[41] has been calculated using NRT analysis, an inbuilt function in NBO 6.0 program.

The HFIP sample (≥99%) was bought from Aldrich and was used without further purification. The mono-deuterated isotope of water (HOD) was prepared by mixing D_2O (99.9% bought from Cambridge Isotope Laboratory) and H_2O in 1:1 molar ratio. Helium gas was used as carrier gas since the signal was more intense with helium gas than with argon gas. Helium gas was bubbled through two separate bubblers, 1 % through a bubbler filled with HFIP and 2 % through a bubbler filled with H_2O. The output of these two bubblers and the carrier gas (97 %) were mixed at a junction leading to the cavity. A pulsed nozzle Fourier transform microwave spectrometer (PNFTMW) was used to record the rotational spectrum, the details of which have been published earlier.[42,43] Multiple free induction decays (FIDs) were recorded per gas pulse. A microwave pulse of 1.0 μs duration was found to be optimum for both the *b*-type and *c*-type transitions. No *a* type transitions were observed.

Results and Discussion

Structure optimization of global and local minima

In the guess geometries, both AP and SC conformers of HFIP were taken into account, though our earlier investigations on HFIP monomer showed that SC conformer did not exist in supersonic expansion.[9] The SC conformer is 4.7 kJ mol^{-1} higher in energy than the AP conformer at MP2/6-311++G(d,p) level of theory. Finally, two structures converged to minima at the same level of theory, one each for AP and SC conformers (Figures 2a and 2c). The structures were confirmed to be minima by frequency calculations at the same level of theory, used for the optimization. To our surprise, binding energy for HFIP(SC)•••water (Figure 2c) complex was 3.8 kJ mol^{-1} greater than that of HFIP(AP)•••water (Figure 2a) and the hydrogen bond distance is about 1.8 Å for both complexes (Table 1). This value suggests a very strong hydrogen bonding between HFIP(SC) and water. During the literature survey, we came across another structure which was identified from a molecular dynamics study (Figure 2b).[44] This structure has HFIP in the AP form and two hydrogen bonds which lead to a five membered stable cyclic structure. In this structure, the C-H group of HFIP forms a C-H•••O hydrogen bond with oxygen of water and the O-H group of H_2O forms O-H•••O hydrogen bond with oxygen of HFIP. However, both hydrogen bonds are bent and quantum calculations show that this structure is less

stable than Structure 2a. All three structures were considered in assigning the experimental spectrum.

The fact that SC conformer was forming a more strongly bound complex with H_2O was intriguing. Would this be the global minimum for this complex? In order to address this, the total electronic energies of all three structures were compared with the binding energy with and without BSSE error. These are given in Table 2. Clearly, the total electronic energy of Structure 2a is 0.9 kJ mol^{-1} lower than that of Structure 2c and therefore Structure 2a is the global minimum in the potential energy hypersurface. It is also worth emphasising that the relative binding energies of the three conformers do show some subtle differences on BSSE corrections.

As the energy differences are small, we have also calculated Gibbs free energy for the monomers and complex at MP2/6-311++G** level of theory (Table 1). This was done at 5 K temperature and 10^{-5} mbar pressure conditions. These conditions are typical for our supersonic molecular beam experiment. When we fed these conditions to G09 program, it considered the pressure as zero and the temperature was kept the same i.e. 5 K. Results at these conditions and their comparisons with the binding energy are given in the Table 1. Change in the free energy and change in the enthalpy on complex formation are calculated using supermolecular approach, similar to the binding energy. It is clear from the table that trends in the change in free energy on complex formation, change in enthalpy on complex formation and change in electronic energy on complex formation are all similar (within 1-2 kJ mol^{-1}) and they do not alter the relative energies of the different conformers. Not surprisingly, the absolute value of the Gibbs energy for the three conformers follow the same trend as the total electronic energy i.e. the global minimum remains Structure 2a even when considering the Gibbs energy surface. Results are given in supporting information, Table S5.

From a rotational spectroscopic point of view, we expected to observe all three *a*-, *b*- and *c*-type of transitions for all the structures, as all three dipole moment components are non-zero. The calculated rotational constants are very similar for the three structures (Table 1). Isotopic substitution studies are used to confirm the structure corresponding to the observed spectrum.

Rotational Spectra and Analysis

Rotational transitions were first searched for the most stable structure 2a. The early searches were made for the selected *b*-type transitions *e.g.* $5_{1,5}$, → $6_{0,6}$, $5_{0,5}$→ $6_{1,6}$, $6_{1,6}$→$7_{0,7}$, $6_{0,6}$→ $7_{1,7}$ etc. Rotational transitions could be observed within 10-20 MHz range of predictions which implied that the predictions were very good. After getting few transitions, they were fitted to rotational Hamiltonian and it was easy to predict the other transitions. We got a progression of 47 transitions soon (Table S6, †ESI). Out of these 47, there were 36 *b*-type and 11 *c*-type transitions. These transitions could be fitted with a semi-rigid rotor Watson's S-reduction asymmetric Hamiltonian within experimental uncertainties (Table 3). The RMS deviation for the fit was 4.3 kHz. With the help of well fitted rotational and distortion constants, *a*-type transitions were predicted and searched for. However, none of the targeted signals could be found. We also considered the possibilities of splitting in *a*-type transitions because of some hindered rotation or tunneling motion and performed long range searches. These searches again did not yield any transitions. These searches covered the regions in which all three structures would have rotational transitions. Reason behind the absence of *a*-type signals is discussed later in details. During experiments, it has been observed that *b*-type transitions were always more intense than *c*-type transitions. This observation was consistent with calculated dipole moment components of structure 2a and 2c while the trend is reverse for structure 2b i.e. *c*-dipole moment is more than *b*-dipole moment (Table 1). Therefore, on the basis of signal intensity, structure 2a or 2c is likely to be the experimentally observed structure. More evidences supporting the structure 2a are given in the following paragraphs.

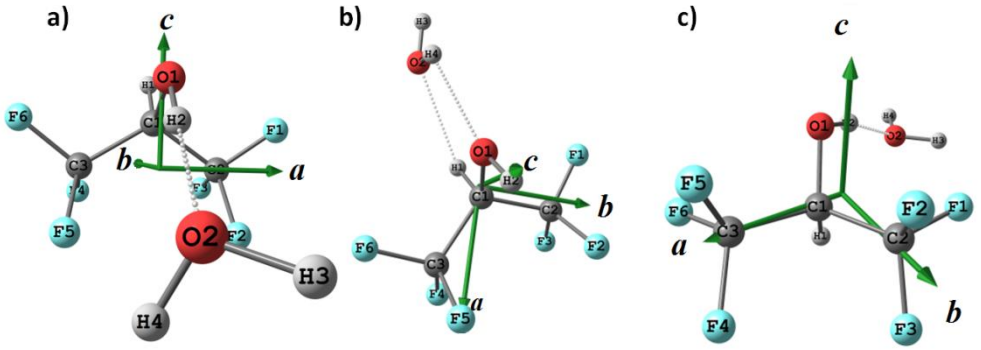

Figure 2. Minima structures for the HFIP•••H_2O complex, obtained at the MP2/6-311++G** level

Table 1. Binding energy, thermodynamic properties, rotational constants, dipole moment and hydrogen bond length of the structures shown in Figure 2a, 2b and 2c.

	Structure 2a	Structure 2b	Structure 2c
Binding Energy (BSSE corrected) in kJ mol^{-1}			
LC-wPBE/6-311++G(d,p)	-31.8	-17.5	-36.8
MP2/6-311++G(d,p)	-28.8	-18.0	-34.3
Thermodynamic Properties at MP2/6-311++G(d,p) in kJ/mol			
Δ(Electronic Energy)*	-40.2	-25.3	-43.9
Δ(Enthalpy)*	-32.7	-19.7	-35.7
Δ(Gibbs free energy)*	-31.7	-18.7	-34.6
Rotational Constants (in MHz) at LC-wPBE/6-311++G(d,p)			
A/MHz	1148.0	1053.5	1249.6
B/MHz	986.9	980.6	845.9
C/MHz	709.2	676.2	636.4
Dipole Moment components at LC-wPBE/6-311++G(d,p)			
$\mu_{a/D}$	0.5	1.9	5.6
$\mu_{b/D}$	1.8	0.2	1.8
$\mu_{c/D}$	1.6	1.6	1.5
Hydrogen bond length (in Å) at LC-wPBE/6-311++G(d,p)			
O•••H distances	1.78	2.23, 2.28[#]	1.80

* Δ denotes the difference between complex value and sum of the monomers values. [#] The structure 2b has two weak hydrogen bonds, C-H•••O and O-H•••O.

Table 2. Comparison between electronic energy and binding energy. All calculations are reported at MP2/6-311++G(d,p) level of theory. The electronic energy for HFIP (AP), HFIP (SC) and water are -788.35601, -788.35423 and -76.27492 Hartree.

	Total Electronic Energy comparison		Binding Energy comparison	
Str	Electronic Energy (Hartree)	Relative energy (kJ mol^{-1})	Relative energy (kJ mol^{-1})	Relative energy corrected for BSSE (kJ mol^{-1})
2a	-864.64624	0.0	0.0	0.0
2b	-864.64058	14.9	14.9	10.8
2c	-864.64589	0.9	-3.8	-5.5

As experimental rotational constants were close for all structures 2a, 2b and 2c, it was difficult to confirm whether experimental rotational constants correspond to structure 2a, 2b or 2c. On initial comparison, we note that experimental rotational constants are closer to those of structure 2a compared to those of Structures 2b or 2c. However, the agreement between experimental and calculated centrifugal distortion constants helped in assigning the structure. Structure 2a has the same sign and magnitude (in order) of the experimental distortion constants (Table 3) whereas both structures 2b and 2c have opposite signs for distortion constants. Thus, the experimentally measured rotational and centrifugal distortions constants support Structure 2a. No transitions could be assigned for Structure 2b and 2c.

Table 3. Experimental rotational and distortion constants, and their comparison with calculated rotational and distortion constants for the structures 2a, 2b and 2c at LC-wPBE/6-311++G(d,p) level of theory.

	Experimental	Calculated Structure 2a	Calculated Structure 2b	Calculated Structure 2c
A/MHz	1134.53857(76)	1147.98533	1053.47733	1250.22042
B/MHz	989.67602(45)	986.88906	980.62909	845.79343
C/MHz	705.26603(21)	709.22576	676.23923	636.52763
D_J/kHz	-0.0855(51)	-0.0291	0.5969	0.2277
D_{JK}/kHz	2.200(36)	1.541	-2.0501	-0.4335
D_K/kHz	-1.783(27)	-1.202	2.8820	1.6368
D_1/kHz	0.0095(28)	0.0015	-0.2418	-0.0493
D_2/kHz	-0.0723(17)	-0.0502	0.0315	0.0051
RMS/MHz	0.0043	--	--	--
No. of transitions	47			

In order to get more accurate structural information, three isotopologues of the titled complex, HFIP•••D_2O, HFIP•••HOD, and HFIP(OD)•••H_2O, have been studied. Predictions for the rotational transitions of the isotopologues were done by comparing the theoretical and experimental rotational constants of the parent complex, and we assumed similar differences in the rotational constants for the isotopologues. We first searched for HFIP•••D_2O complex since both HFIP and D_2O were available in pure form and spectrum could be observed easily. A total of 30 transitions, mostly *b*-type transitions were observed for the HFIP•••D_2O complex (Table S7, †ESI). Two rotational transitions, corresponding to the HFIP•••D_2O isotopologue, are shown in Figure 3. The presented signals are at frequencies 7178.7880 and 7179.0490 MHz and are assigned as $4_{14} \rightarrow 5_{05}$ and $4_{04} \rightarrow 5_{15}$ transitions, respectively for HFIP•••D_2O. The next search was performed for HFIP•••HOD isotopologue and we could observe 36 transitions (Table S8, †ESI) which include 31 b-type and 5 c-type transitions. Splitting in rotational transitions because of deuterium quadruple moment has been seen in some signals. However, these were insufficient to assign and measure the quadruple coupling constant of deuterium. Line centers were used in the fit. Searches for HFIP(OD)•••H_2O isotopologue was performed finally and we could observe 10 transitions (Table S9, †ESI). Transitions corresponding to each isotopologue were fitted to the semi-rigid rotational Hamiltonian. The d1 and d2 distortion constants for HFIP(OD)•••H_2O complex and d1 distortion constant HFIP•••HOD complex were not determined well. Therefore, distortion constants of the parent complex were used and kept constant during the fit. The experimental rotational and distortion constants of all isotopologues are given in Table 4. The RMS values for these fits were 3.5, 4.3 and 5.1 kHz for HFIP•••D_2O, HFIP•••HOD and HFIP(OD)•••H_2O isotopologues, respectively. Like for the parent complex, *b*-type transitions were stronger than *c*-type transitions for all isotopologues.

Using Kraitchmann's analysis, the location of the isotopically substituted atoms could be determined. These could be compared with the theoretical predictions for the three

different structures in order to provide further confirmation of the structure. As several levels of calculations have been carried out, we compared the experimental rotational and distortion constants with those determined at various levels, see Table 5. We note that the results at the LC-wPBE/6-311++G(d,p) level of calculations match the experimental values very closely. Hence, it was decided to compare the structural results from this level of calculations with the results from Kraitchman's analysis. Results are given in Table 6. The experimentally determined distances were close to those of structure 2a. This analysis confirmed that the observed structure is structure 2a. We found other interesting outcomes from the isotopologues study, presented in the next paragraphs.

In the ab initio calculated structure 2a, both hydrogen atoms of water molecule are not equivalent in its equilibrium structure. Therefore, two sets of progression were expected for the HFIP•••HOD isotopologue. However, we observed only one progression experimentally which suggests that the two water hydrogen atoms are equivalent in their vibrationally averaged structure and the complex has a plane of symmetry. A possible motion which can make the structure symmetric, on an average, is the partial rotation of H_2O about its c-axis. This reversed the sign of *a*-dipole. A relaxed potential energy scan has been performed for this motion at the LC-wPBE/6-311++G(d,p) level of theory (Figure 4). The dihedral angle C2-C1-O2-H3 (see Figure 2a) was chosen for the scan and the selected range was -30° to 30°. The normal mode vibrational frequency which mimics the above mentioned motion, was 74 cm^{-1} at LC-wPBE/6-311++G(d,p) level of theory. The zero point energy (ZPE) 0.46 kJ mol^{-1} for this normal mode vibrational motion was higher than the barrier obtained from the dihedral angle scan (0.25 kJ mol^{-1}). It suggests that this motion is free and both the hydrogen atoms are equivalent in the zero-point averaged dynamic structure of the complex. Due to this free motion, *a*-dipole component averages out and this could explain the absence of *a*-type transitions.

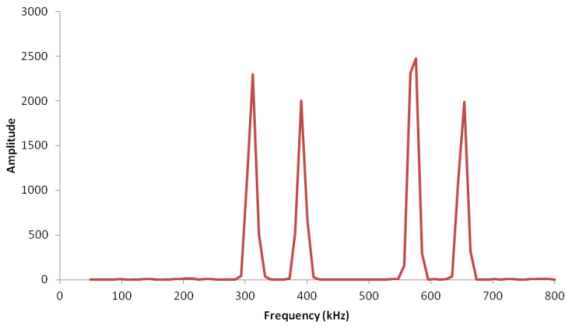

Figure 3. A sample spectrum of the HFIP•••D_2O complex. This figure contains two transitions. First and second peaks are the two Doppler components of one of the signals. Similarly third and fourth are the two Doppler components of the other signal. The molecular frequencies corresponding to these signal are 7179.049 MHz and 7178.788 MHz and are assigned as $4_{14} \rightarrow 5_{05}$ and $4_{04} \rightarrow 5_{15}$ respectively.

Table 4. Rotational and distortion constants for three different isotopologues.

	HFIP•••D_2O	HFIP•••HOD	HFIP(OD)•••H_2O
A/MHz	1075.1262(10)	1110.15566(49)	1126.482(30)
B/MHz	983.0710(16)	986.04212(71)	988.2787(82)
C /MHz	683.64615(22)	696.72957(18)	702.7647(25)
D_J /kHz	-0.148(25)	-0.1752(63)	-0.209(33)
D_{JK} /kHz	2.43(16)	3.548(78)	11.1(13)
D_K /kHz	-1.91(14)	-2.999(77)	-6.7(16)
d_1 /kHz	0.029(11)	[0.0095]*	[0.0095]*
d_2 /kHz	-0.0861(57)	-0.1220(32)	[-0.0723]*
RMS /MHz	0.0035	0.0043	0.0051
No of transitions	30	37	10

*Value in square brackets is taken from the constants of the parent complex and kept constant during fit.

Table 5. Comparison of experimental and calculated rotational constants (MHz) and distortion constant (kHz).

	Experiment	#MP2	MP2=full	B2PLYP	B2PLYPD	LC-wPBE	CAM-B3LYP	wB97XD	#MP2/6-31G(d)
A/MHz	1134.53898(77)	1148.3	1151.0	1142.9	1170.2	1148.0	1164.7	1165.4	1187.6
B/MHz	989.67594(44)	986.2	988.5	977.9	979.8	986.9	982.9	977.3	985.9
C/MHz	705.26602(20)	710.5	712.4	704.9	719.3	709.2	715.2	714.1	734.6
D_J/MHz	-0.0876(51)	-0.007	-0.007	0.005	-0.004	-0.029	0.010	-0.010	-0.056
D_{JK}/MHz	2.230(39)	1.144	1.135	1.116	1.007	1.542	1.018	1.142	1.680
D_K/MHz	-1.805(29)	-0.869	-0.864	-0.795	-0.800	-1.203	-0.756	-0.865	-1.478
d_1/MHz	0.0092(27)	-0.003	-0.003	-0.004	0.001	0.002	-0.005	-0.0001	-0.003
d_2/MHz	-0.0738(18)	-0.038	-0.038	-0.037	-0.030	-0.050	-0.033	-0.035	-0.050

Basis set used for all the calculations is 6-311++G(d,p) except last column. At MP2/6-31G(d) level, both hydrogen atoms of water are equivalent.

Journal Name

ARTICL

Table 6. Parameters for the different conformers of HFIP•••H2O complex from Kraitchman's analysis and ab initio calculations at LC-wPBE/6-311++G(d,p) level of theory.

Distances	Experimental	Calculated Structure 2a	Calculated Structure 2b	Calculated Structure 2c
CM-H1/Å	3.19588(83)	3.175	3.229	3.870
CM-H2/Å)	3.88827(70)	3.709	4.303	4.455
CM-H3/Å)	1.7962(34)	1.885	2.043	2.211

*CM stands for centre of mass and H1 and H2 are the hydrogen of water molecule and H3 is the bonded hydrogen in complex.

The above analysis suggests that there is an effective plane of symmetry and the two hydrogen atoms in H_2O are dynamically equivalent. This contradicts the results from Kraitchmann's analysis discussed above. For HFIP•••H_2O complex, the calculated distances between center of mass (CM) to H1 and H2 (both are water hydrogen atoms) were 3.17 Å and 3.71 Å, respectively, in its equilibrium structure. These are in reasonable agreement with the results from Kraitchmann's analysis, 3.196 Å and 3.888 Å, though this analysis is not expected to be reliable for H/D substitution. We note that, in the calculated vibrationally averaged geometry, these distances are 3.41 Å and 3.65 Å, respectively. Clearly the difference in distances for the two H atoms is reducing.

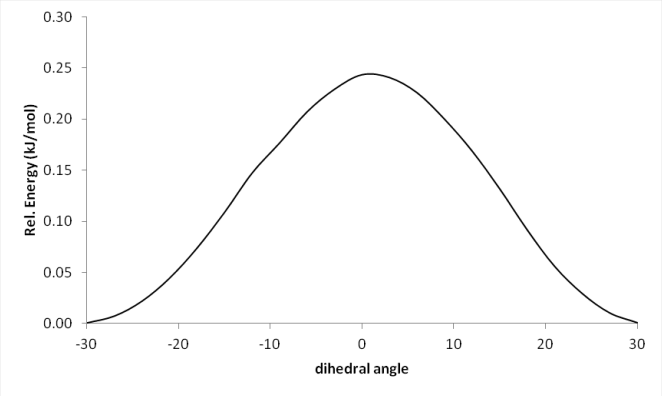

Figure 4. Relaxed PES scan of C2-C1-O2-H3 dihedral angle (see Figure 2a) at the LC-wPBE/6-311++G(d,p) level.

AIM analysis

For structure 2a and 2c, the calculated hydrogen bond length was very short, 1.8 Å and it can be considered as a very strong O•••H-O hydrogen bond. In general there is a strong correlation between electron density at BCPs and binding energies. The electron density value at the BCP is 0.0348 and 0.0332 a.u. for O•••H-O hydrogen bond in the structure 2a and 2c, respectively (Figure 5). These values also suggest that structure 2a is more stable than structure 2c. Note that the structure 2a appeared as global minima based on total electronic energy calculation. For water dimer, the electron density value at O•••H-O hydrogen bond is 0.0241 a.u. These numbers indicate that the O-H•••O hydrogen bonding in structure 2a and 2c are stronger than that in water dimer. Water dimer is a simple example of O•••H-O interaction and information about the complex is well established using different theories and experiments. Qualitatively, structure 2a and 2c should be stronger than the water dimer because of two electron withdrawing groups, CF_3 which makes the OH hydrogen more acidic (electrophilic). For structure 2b, two BCPs were found and electron density values at BCPs are 0.0132 a.u. and 0.0137 a.u. (Figure 5). Structure 2a or 2c which has only one intermolecular hydrogen bond BCP is even more stable than structure 2b even though this structure has two hydrogen bond BCPs. The sum of the electron densities at these two BCPs of structure 2b is less than the electron density value at the hydrogen bond BCP of structure 2a or 2c. Moreover, structure 2a has three more BCPs, one between two fluorine atoms and two similar BCPs between two different F and O (Figure 5). If BCPs are very close to ring critical point (RCP), bonds are considered to be very weak (unstable). In Figure 5, all three BCPs are close to RCPs in structure 2a. In structure 2b, one F•••F BCP is present and it is close to a RCP. In structure 2c, one F•••F and one O•••F BCPs are present and near to RCPs. We will discuss later about these unexpected BCPs.

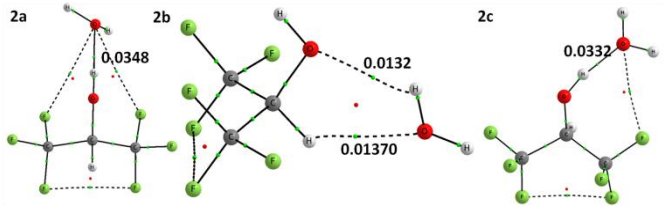

Figure 5. AIM analysis of the structures, green and red dots are BCPs and RCPs, respectively. Electron densities values (in a.u.) are presented at the intermolecular hydrogen bond.

The AIM theory can also be used to understand the nature of interactions, whether it is a closed-shell interaction i.e. ionic bond or a shared-shell interaction i.e. covalent bond. Initially, the sign of Laplacian of the electron density[45] was used to characterize the interaction as closed or shared shell. Laplacian at BCP is the summation of three Eigenvalues (λ_1, λ_2 and λ_3) of the Hessian matrix of electron density. If it is positive, the interaction is closed-shell and if it is negative the interaction is

shared-shell. It was noted that this could lead to erroneous results.[46] Recently several other parameters such as |V|/G ratio[47], H-values,[46] and $|\lambda_1|/\lambda_3$ ratio[48] at the BCP have been introduced to address this question. V, G and H are the potential, kinetics and total (V+G) electron energy density at BCP, respectively. For closed-shell and shared-shell interactions, |V|/G < 1 and |V|/G > 2, respectively. For the intermediate type of bonding, |V|/G ratio values fall between one and two. Positive or negative H-value defines the closed-shell or shared shell interaction, respectively. If the values of $|\lambda_1|/\lambda_3$ ratio is less than 0.25, it is considered as closed-shell interaction.[41] For structure 2a, Laplacian has a positive sign (+0.1225 a.u.), V/G ratio is 0.99, H-value is 0.0001 a.u., and $|\lambda_1|/\lambda_3$ ratio is 0.24. All these values indicate that the intermolecular interaction in structure 2a is a very strong closed-shell interaction and mostly lies near the boundary of shared-shell and closed-shell interaction.[41]

NBO analysis

In contrast to AIM analysis, NBO analysis of structure 2a did not show orbital overlapping for some of the mentioned BCPs but it showed an overlap between lone pair of water and O-H antibonding orbital of HFIP which leads to the formation of hydrogen bond and stabilizes the complex by 87.7 kJ mol^{-1}. In structure 2c the same overlapping results in 73.8 kJ mol^{-1} stabilization. It may be noted that, NBO also supports that the structure 2a is more stable than structure 2b, like total electronic energy comparison. In structure 2b, overlapping of oxygen's lone pair of water with C-H antibonding of HFIP stabilizes the complex by 7.52 kJ mol^{-1} and second overlapping of oxygen's lone pair of HFIP with O-H antibonding of HFIP stabilizes the complex by 3.68 kJ mol^{-1}. These values again indicate that hydrogen bond in structure 2a is most stable. For structure 2a, NRT analysis confirmed that 0.88% resonance structure (0.02% covalent and 0.86% ionic) has hydrogen bond (O2•••H2). For structure 2c, the hydrogen bond has 0.74% ionic and 0.01% covalent character. It is well known that the deviation from 180° of O•••H-O hydrogen bond angle results in weakening of the hydrogen bond.[49] In structure 2a, O•••H-O bond angle is 180° while in structure 2b, they are 125 and 123°. Non linear hydrogen bond angles of structure 2b were reason for the lower stability of this complex.

NCI analysis

We wanted to confirm whether unexpected BCPs are the artifact of AIM theory or it is some real interaction. We found that the NBO analysis did not show any specific overlap corresponding to these BCPs. We used another recent method, NCI plot,[23] which could determine these interactions (Figure 6). This method is able to determine the very weak intramolecular interaction in 1,2-ethanediol which is not identified through BCP.[50] Recently, we have also determined a very weak intra-molecular interaction in N,N-diphenyloxamide derivatives using this method and AIM theory did not show BCP for this interaction.[51] In the figure 6, sign(λ2)*ρ is plotted as function 1 on x-axis and its negative values imply attractive interaction (hydrogen bond, halogen bond or van der Waals interaction) whereas positive values imply repulsive interaction (steric effect). On y-axis, the reduced density gradient (RDG) values are plotted as function 2 and it is derived from the gradient of electron density. Readers are referred to Ref. 23 for the details of this method. Both these functions have information about weak interaction and clubbing them makes a powerful method to probe attractive and repulsive interactions. In Figure 6, a peak around -0.035 represents strong (H2•••O2) hydrogen bonding in structure 2a. Other four peaks which have negative values near zero, denote F2•••O2, F5•••O2, F3•••F4, F2•••F5 interactions (see figure 2a). No BCP was found for the F2•••F5 interaction but this interaction is revealed only by NCI plot. Values show that these interactions are very weak. For structure 2c, the peak around -0.033 represent a stronger (H2•••O2) hydrogen bonding. However, this bond is weaker than that of the hydrogen bond present in structure 2a. Moreover, three attractive interactions (F1•••O2, F3•••F4 and F2•••F5) are also present in the structure 2c. Similarly, for structure 2b, NCI plot shows many peaks corresponding to attractive and repulsive interactions. For clear visualization of these interactions in molecular frame, color-filled RDG values are plotted in Figure 7. Overall, there are five attractive and four repulsive interactions in structure 2a, six attractive and five repulsive interactions in structure 2b and four attractive and three repulsive interactions in structure 2c (Figure 7).

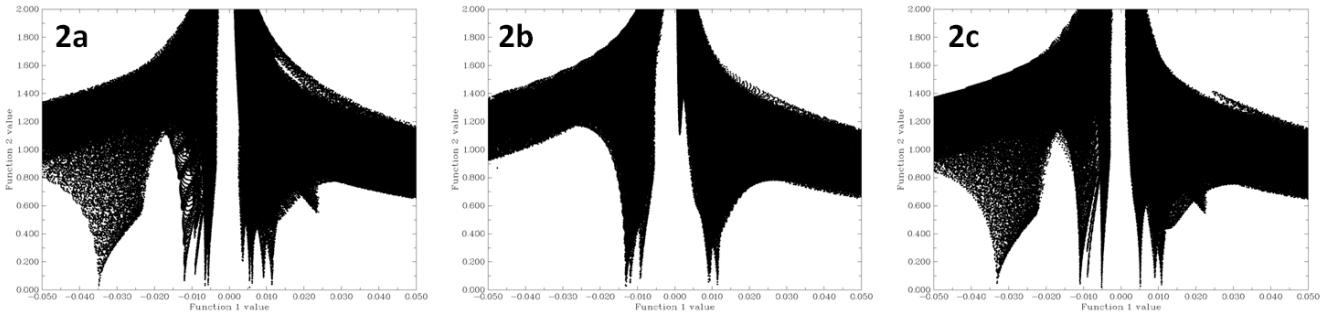

Figure 6: NCI index plot. Left side and right side figures correspond to Structure 2a and Structure 2b, respectively. On x-axis, sign(λ2)*ρ values and on y-axis, RDG values are plotted as function 1 and function 2, respectively.

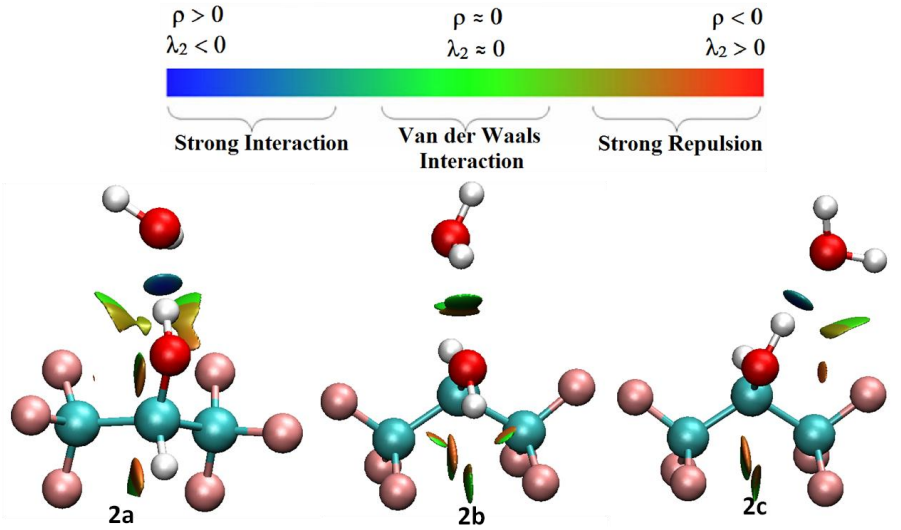

Figure 7: Color-filled RDG isosurface plot. Left side and right side figures correspond to Structure 2a and Structure 2b, respectively.

Conclusion

The most stable structure (structure 2a) of HFIP•••water complex was determined using PNFTMW spectrometer. Monomer HFIP can exist in the form of two conformers, AP and SC. The AP conformer is more stable than the SC conformer. Ab initio calculation predicted three structures for the complex. Microwave spectrum identified only one of the three structures and this happens to be the global minimum in the potential energy hypersurface. This structure has the OH group in HFIP(AP) forming a strong hydrogen bond with the O atom from H_2O. Moreover, AIM, NBO, and NCI index analyses also predict structure 2a to be the global minimum.

The rotational constants for all three structures were similar. However, centrifugal distortion constants and the Kraitchman analysis based on three isotopologues, HFIP•••D_2O, HFIP•••HOD, and HFIP(OD)•••H_2O provided positive confirmation of the structure. Moreover, the fact that *b*-type transitions were stronger than *c*-type transitions is consistent with the structure 2a. Absence of the expected *a*-type transitions can be explained on the basis of the partial rotation of water along *c*-axis. The barrier for this motion was much lower than the ZPE of corresponding normal mode vibration. This free motion also explains the dynamical equivalence of the two hydrogen atoms of water in the complex.

The HFIP•••water complex has a stronger hydrogen bond than the water dimer. In addition, AIM and NCI analyses discovered some more attractive interactions in all structures. These include intramolecular interaction between F atoms in the two CF_3 groups and also intermolecular interaction between the O atom of H_2O and two F atoms in the two CF_3 groups. Finally, we note that the LC-wPBE/6-311++G** method works better than many other methods for the HFIP-H_2O complex.

Acknowledgements

The authors thank the Indo-French Centre for Promotion of Advanced Scientific Research for partial support. The Authors also thank the Super Computer Research Center and Inorganic and Physical Chemistry department at the Indian Institute of Science for providing good computational facilities. A. S. thanks Council for Research and Industrial Research (CSIR), of India for the fellowship and Dr. Devendra Mani for his help during experiments.

References

1. M. Rosenblatt, N. V Beaudette, and G. D. Fasman, *Proc. Natl. Acad. Sci. U. S. A.*, 1980, **77**, 3983–3987.
2. D. P. Hong, M. Hoshino, R. Kuboi, and Y. Goto, *J. Am. Chem. Soc.*, 1999, **121**, 8427–8433.
3. S. Bhattacharjya, J. Venkatraman, A. Kumar, and P. Balaram, *J. Pept. Res.*, 1999, **54**, 100–111.
4. R. Rajan and P. Balaram, *Int. J. Pept. Protein Res.*, 1996.
5. S. J. Ferrito, in *Encyclopedia of Chromatography, Second Edition*, 2011.
6. M. Burdisso, R. Gandolfi, L. Toma, and R. Obertib, *Tetrahedron*, 1991, **47**, 6725–6736.
7. K. Yoshida, T. Yamaguchi, T. Adachi, T. Otomo, D. Matsuo, T. Takamuku, and N. Nishi, *J. Chem. Phys.*, 2003, **119**, 6132–6142.
8. B. Czarnik-Matusewicz, S. Pilorz, L.-P. Zhang, and Y. Wu, *J. Mol. Struct.*, 2008, **883-884**, 195–202.
9. A. Shahi and E. Arunan, *J. Phys. Chem. A*, 2015, **119**, 5650–5657.
10. J. R. Durig, R. A. Larsen, F. O. Cox, and B. J. van der Veken, *J. Mol. Struct.*, 1988, **172**, 183–201.
11. J. Murto, A. Kivinen, R. Viitala, and J. Hyömäki, *Spectrochim. Acta Part A Mol. Spectrosc.*, 1973, **29A**, 1121–1137.
12. A. J. Barnes and J. Murto, *J. Chem. Soc., Faraday Trans. 1*, 1972, **68**, 1642–1651.
13. H. Schaal, T. Häber, and M. A. Suhm, *J. Phys. Chem. A*, 2000, **104**, 265–274.
14. K. F. Purcell, J. A. Stikeleather, and S. D. Brunk, *J. Mol. Spectrosc.*, 1969, **32**, 202–213.
15. S. J. Cyvin, J. Brunvoll, and M. Perttilä, *J. Mol. Struct.*, 1973, **17**, 17–21.
16. E. Hirota and Y. Kawashima, *J. Mol. Spectrosc.*, 2001, **207**, 243–253.

17. S. Kondo and E. Hirota, *J. Mol. Spectrosc.*, 1970, **34**, 97–107.
18. G. S. Grubbs, S. E. Novick, W. C. Pringle, J. Laane, E. J. Ocola, and S. A. Cooke, *J. Phys. Chem. A*, 2012, **116**, 8169–8175.
19. D. A. Obenchain, D. J. Frohman, G. S. Grubbs II, B. E. Long, W. C. Pringle, and S. E. Novick, *Talk TC04, 67th Int. Symp. Mol. Spectrosc. Ohio State Univ. Columbus, OH.*, 2012.
20. R. F. W. Bader, *Atoms in Molecules: A Quantum Theory*, Clarendon Press, Oxford, 1990.
21. P. L. A. Popelier, *Atoms in Molecules. An Introduction*, Pearson Education Ltd. Essex, England, 2000.
22. A. E. Reed, L. A. Curtiss, and F. Weinhold, *Chem. Rev.*, 1988, **88**, 899–926.
23. E. R. Johnson, S. Keinan, P. Mori-Sánchez, J. Contreras-García, A. J. Cohen, and W. Yang, *J. Am. Chem. Soc.*, 2010, **132**, 6498–6506.
24. E. D. Glendening and F. Weinhold, *J. Comput. Chem.*, 1998, **19**, 593–609.
25. E. D. Glendening and F. Weinhold, *J. Comput. Chem.*, 1998, **19**, 610–627.
26. E. D. Glendening, J. K. Badenhoop, and F. Weinhold, *J. Comput. Chem.*, 1998.
27. S. R. Gadre and P. K. Bhadane, *J. Chem. Phys.*, 1997, **107**, 5625–5626.
28. P. Politzer and J. S. Murray, *Chemphyschem*, 2013, **14**, 278–294.
29. T. Lu and F. Chen, *J. Comput. Chem.*, 2012, **33**, 580–592.
30. T. Lu and F. Chen, *J. Mol. Graph. Model.*, 2012, **38**, 314–323.
31. M. J. Frisch, G. W. Trucks, H. B. Schlegel, G. E. Scuseria, M. A. Robb, J. R. Cheeseman, G. Scalmani, V. Barone, B. Mennucci, G. A. Petersson, H. Nakatsuji, M. Caricato, X. Li, H. P. Hratchian, A. F. Izmaylov, J. Bloino, G. Zheng, J. L. Sonnenberg, M. Hada, M. Ehara, K. Toyota, R. Fukuda, J. Hasegawa, M. Ishida, T. Nakajima, Y. Honda, O. Kitao, H. Nakai, T. Vreven, J. A. Montgomery Jr., J. E. Peralta, F. Ogliaro, M. Bearpark, J. J. Heyd, E. Brothers, K. N. Kudin, V. N. Staroverov, R. Kobayashi, J. Normand, K. Raghavachari, A. Rendell, J. C. Burant, S. S. Iyengar, J. Tomasi, M. Cossi, N. Rega, J. M. Millam, M. Klene, J. E. Knox, J. B. Cross, V. Bakken, C. Adamo, J. Jaramillo, R. Gomperts, R. E. Stratmann, O. Yazyev, A. J. Austin, R. Cammi, C. Pomelli, J. W. Ochterski, R. L. Martin, K. Morokuma, V. G. Zakrzewski, G. A. Voth, P. Salvador, J. J. Dannenberg, S. Dapprich, A. D. Daniels, O. Farkas, J. B. Foresman, J. V Ortiz, J. Cioslowski, and D. J. Fox, *Gaussian:09 Revision D.01*, Gaussian, Inc., Wallingford, CT, 2009.
32. O. A. Vydrov and G. E. Scuseria, *J. Chem. Phys.*, 2006, **125**, 234109.
33. J.-D. Chai and M. Head-Gordon, *Phys. Chem. Chem. Phys.*, 2008, **10**, 6615–20.
34. S. Grimme, *J. Chem. Phys.*, 2006, **124**, 034108.
35. W. Gordy and R. L. Cook, *Microwave Molecular Spectra. 2nd ed.*, New York: Wiley Interscience, 1984.
36. H. M. Pickett, *J. Mol. Spectrosc.*, 1991, **148**, 371–377.
37. Z. Kisiel, *PROSPE - Programs for rotational spectroscopy*, http://info.ifpan.edu.pl/~kisiel/prospe.htm.
38. Z. Kisiel, in *Spectroscopy from Space SE - 6*, eds. J. Demaison, K. Sarka, and E. Cohen, Springer Netherlands, 2001, vol. 20, pp. 91–106.
39. T. A. Keith, *AIMAll (Version 14.11.23), Todd A. Keith, TK Gristmill Software, Overl. Park KS, USA, 2013*, 2014.
40. E. D. Glendening, J. K. Badenhoop, A. E. Reed, J. E. Carpenter, J. A. Bohmann, C. M. Morales, C. R. Landis, and F. Weinhold, *NBO 6.0 program*, Theoretical Chemistry Institute, University of Wisconsin, Madison, WI, USA, 2013.
41. A. Shahi and E. Arunan, *Phys. Chem. Chem. Phys.*, 2014, **16**, 22935–22952.
42. E. Arunan, A. P. Tiwari, P. K. Mandal, and P. C. Mathias, *Curr. Sci.*, 2002, **82**, 533–540.
43. E. Arunan, S. Dev, and P. K. Mandal, *Appl. Spectrosc. Rev.*, 2004, **39**, 131–181.
44. T. Yamaguchi, S. Imura, T. Kai, and K. Yoshida, *Zeitschrift für Naturforsch. A*, 2013, **68a**, 145–151.
45. R. F. W. Bader and H. Essen, *J. Chem. Phys.*, 1984, **80**, 1943–1960.
46. D. Cremer and E. Kraka, *Angew. Chemie Int. Ed. English*, 1984, **23**, 627–628.
47. E. Espinosa, I. Alkorta, J. Elguero, and E. Molins, *J. Chem. Phys.*, 2002, **117**, 5529–5542.
48. N. J. M. Amezaga, S. C. Pamies, M. Peruchena, N. M. Peruchena, and G. L. Sosa, *J. Phys. Chem. A*, 2010, **114**, 552–562.
49. E. Arunan, G. R. Desiraju, R. A. Klein, J. Sadlej, S. Scheiner, I. Alkorta, D. C. Clary, R. H. Crabtree, J. J. Dannenberg, P. Hobza, H. G. Kjaergaard, A. C. Legon, B. Mennucci, and D. J. Nesbitt, *Pure Appl. Chem.*, 2011, **83**, 1619–1636.
50. J. R. Lane, J. Contreras-García, J.-P. Piquemal, B. J. Miller, and H. G. Kjaergaard, *J. Chem. Theory Comput.*, 2013, **9**, 3263–3266.
51. A. Lakshmipriya, S. Rama Chaudhari, A. Shahi, E. Arunan, and N. Suryaprakash, *Phys. Chem. Chem. Phys.*, 2015, **17**, 7528–7536.

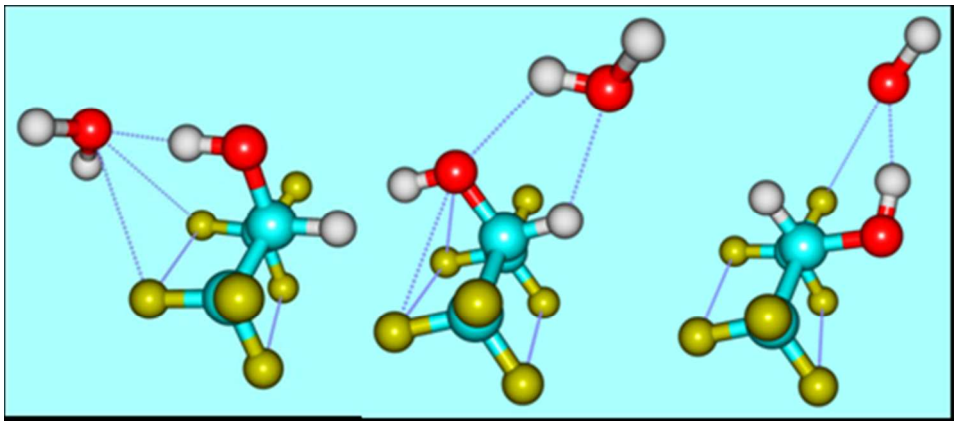

Microwave spectrum of the hexafluoroisopropanol-water complex unambiguously identifies the global minimum in which OH of hxafluoroisopropanol forms a strong hydrogen bond with O from water
80x35mm (150 x 150 DPI)